Edentulism, beaks, and biomechanical innovations in the evolution of theropod dinosaurs

Stephan Lautenschlager[a,1], Lawrence M. Witmer[b], Perle Altangerel[c], and Emily J. Rayfield[a]

[a]School of Earth Sciences, University of Bristol, Bristol BS8 1RJ, United Kingdom; [b]Department of Biomedical Sciences, Heritage College of Osteopathic Medicine, Ohio University, Athens, OH 45701; and [c]Mongolian Museum of Natural History, National University of Mongolia, Ulaanbaatar 21, Mongolia

Edited by Ophir Klein, University of California, San Francisco, CA, and accepted by the Editorial Board November 3, 2013 (received for review June 5, 2013)

Maniraptoriformes, the speciose group of derived theropod dinosaurs that ultimately gave rise to modern birds, display a diverse and remarkable suite of skeletal adaptations. Apart from the evolution of flight, a large-scale change in dietary behavior appears to have been one of the main triggers for specializations in the bauplan of these derived theropods. Among the different skeletal specializations, partial or even complete edentulism and the development of keratinous beaks form a recurring and persistent trend in from the evolution of derived nonavian dinosaurs. Therizinosauria is an enigmatic maniraptoriform clade, whose members display these and other osteological characters thought to be correlated with the shift from carnivory to herbivory. This makes therizinosaurians prime candidates to assess the functional significance of these morphological characters. Based on a highly detailed biomechanical model of *Erlikosaurus andrewsi*, a therizinosaurid from the Upper Cretaceous of Mongolia, different morphological configurations incorporating soft-tissue structures, such as a keratinous rhamphotheca, are evaluated for their biomechanical performance. Our results indicate that the development of beaks and the presence of a keratinous rhamphotheca would have helped to dissipate stress and strain, making the rostral part of the skull less susceptible to bending and displacement, and this benefit may extend to other vertebrate clades that possess rhamphothecae. Keratinous beaks, paralleled by edentulism, thus represent an evolutionary innovation developed early in derived theropods to enhance cranial stability, distinct to postulated mass-saving benefits associated with the origin of flight.

functional morphology | computer modelling | finite element analysis

The evolution from nonavian to avian theropods (birds) is defined by a plethora of anatomical and functional specializations, many of which have been linked to the evolution of flight (1–3). However, several skeletal traits and adaptations, gradually acquired within distinct clades of Maniraptoriformes, appear to have been induced by or sparked dietary diversification (4). Many of these morphological characters are now thought to be closely associated with a trophic shift from carnivory to omnivory or herbivory (5–7) and are regarded as the result of correlated character evolution, occurring independently in three or perhaps as many as five lineages of Maniraptoriformes, suggesting a role of these characters in the functional acquisition of herbivory (4). Most obvious is the trend toward tooth reduction, which ultimately leads to partial or complete edentulism, and is paralleled by the appearance of a beak-like keratinous rhamphotheca. Edentulism has occurred independently multiple times in tetrapod history, usually accompanied by the abandonment of obligate carnivory (8). Apparently freed from functional constraints associated with a carnivorous diet, this permitted diversification of skull and beak shapes, particularly among extant and extinct birds (9). Biomechanical studies on extant birds have indicated a functional benefit of rhamphothecae and beaks other than weight reduction (10, 11). However, the functional role of edentulism and (keratinous) beaks in the evolution of herbivory from a macropredaceous heritage is still unclear.

Therizinosauria—an enigmatic clade of maniraptoriform dinosaurs, restricted to the Cretaceous of Asia and North America—is a prime example for the diverse skeletal modifications occurring in the maniraptoriform bauplan. Their basal position among Maniraptora (12) makes therizinosaurians of special interest in terms of the evolutionary functional relevance of these features. Due to their highly unusual and peculiar skeletal morphology, therizinosaurians have been the focus of many taxonomic and paleoecological controversies since the discovery of the first specimens. Numerous discoveries in recent decades have substantiated therizinosaurians as specialized, even bizarre, theropod dinosaurs (12–14). Derived members of this clade are characterized by a suite of osteological features in the cranial and postcranial skeleton that are highly divergent from those of typically carnivorous theropods, such as (*i*) numerous, small, lanceolate teeth; (*ii*) a medial deflection of the tooth row; (*iii*) an edentulous premaxilla and dentary tip, suggesting the presence of a rostral rhamphotheca; (*iv*) hypertrophied manual unguals; and (*v*) a broad, opisthopubic pelvis.

Triggered by this unusual morphology, in particular of the cranial skeleton, a range of trophic and ecological theories have been proposed over the years. Although the suggested interpretations of dietary behavior for therizinosaurians range from amphibiotic piscivory (15) to terrestrial or arboreal insectivory (16), derived therizinosaurs are now generally regarded as having been predominantly herbivorous (4, 7). Moreover, none of these hypotheses have been tested quantitatively in a functional context.

The therizinosaurid *Erlikosaurus andrewsi*, from the Upper Cretaceous (Cenomanian-Turonian) Baysheen Tsav locality of Mongolia, is the only example of a nearly complete and three-

Significance

Edentulism and beaks (rhamphothecae) are distinguishing features among extant birds and are traditionally regarded as a response to weight-saving demands for the evolution of flight. However, keratin-covered beaks paralleled by edentulism appeared in non-avian theropod dinosaurs and as early as the Early Cretaceous. Here, high-resolution, digital biomechanical models of the skull of the Cretaceous therizinosaur *Erlikosaurus andrewsi* are used to investigate the functional significance of these morphological specialisations and adaptations occurring in non-avian, maniraptoriform dinosaurs. Results of finite-element analyses provide evidence that keratinous beaks play an important role in enhancing cranial stability by mitigation stress and strain during feeding and represent an evolutionary innovation developed early in derived theropod dinosaurs.

Author contributions: S.L., L.M.W., and E.J.R. designed research; S.L. and E.J.R. performed research; S.L., L.M.W., and P.A. contributed new reagents/analytic tools; S.L. and E.J.R. analyzed data; and S.L., L.M.W., and E.J.R. wrote the paper.

The authors declare no conflict of interest.

This article is a PNAS Direct Submission. O.K. is a guest editor invited by the Editorial Board.

Freely available online through the PNAS open access option.

[1]To whom correspondence should be addressed. E-mail: glzsl@bristol.ac.uk.

This article contains supporting information online at www.pnas.org/lookup/suppl/doi:10.1073/pnas.1310711110/-/DCSupplemental.

dimensionally preserved skull of any therizinosaurian (17). Representing the cranial adaptations found across different clades of Maniraptoriformes, it provides a unique opportunity to test the biomechanical behavior of a beaked theropod and to investigate the functional consequences of tooth reduction and the development of a keratinous rhamphotheca: characteristic features, which have a plesiomorphic distribution among Maniraptoriformes and patchy distribution in Mesozoic birds before becoming autapomorphic traits in Neornithine birds (4, 9). Focusing on a single taxon allows controlled hypothesis testing of models of beak evolution without the confounding effects of interspecific differences in geometry. Based on high-resolution CT scans of the original specimen, the cranial skeleton, the jaw adductor musculature, and the keratinous rhamphotheca of *E. andrewsi* (Fig. 1) have been digitally restored in high detail (18).

Here, we perform a functional analysis of the skull and lower jaw of *E. andrewsi*, using detailed simulations of the cranial hard- and soft-tissue structures. Using 3D finite-element analysis (FEA), a computational technique developed to predict the distribution of stress and strain in complex geometric objects, we are able to compare and evaluate the biomechanical performance of different morphological configurations. Alongside the restored morphology, different hypothetical models based on alternative interpretations of osteological correlates are tested. The results of these tests shed light on the functional significance and mechanical benefits of edentulism and a keratinous rhamphotheca, which in turn provides the functional context for interpreting dietary shifts in derived nonavian theropods and birds.

Results

Different morphological configurations were tested for the skull (restored skull without rhamphotheca, skull with small rhamphotheca, skull with large rhamphotheca, and fully dentigerous model) and the lower jaw (restored lower jaw, lower jaw with rhamphotheca) (*SI Appendix*, Tables S1–S3), simulating different biting scenarios (snout tip, rostralmost tooth position, caudalmost tooth position, as well as an intermediate tooth position for the lower jaw). To investigate the effects of the postcranial musculature, further scenarios simulating the action of neck musculature were tested.

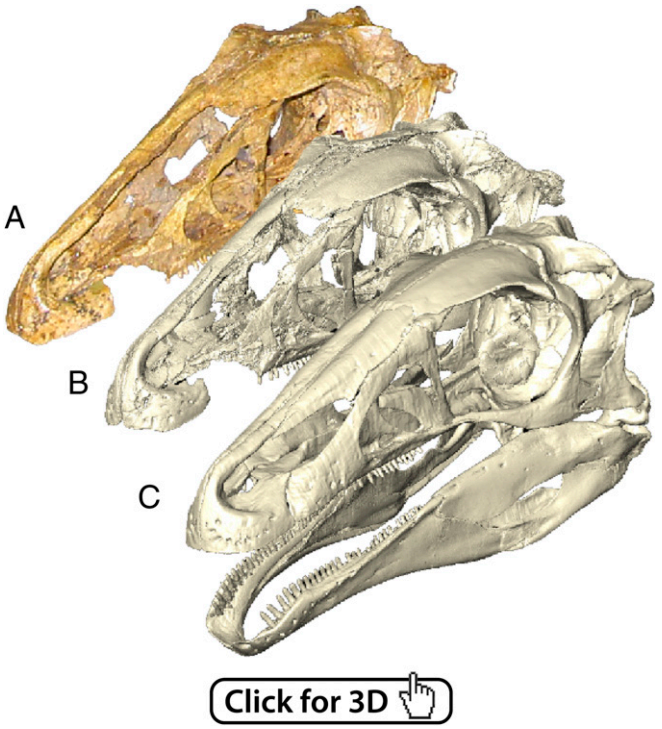

Fig. 1. Reconstructed cranial morphology of *E. andrewsi*. (*A*) Photograph of original (holotype) specimen. (*B*) Digital representation of original specimen. (*C*) Restored morphology used for finite element models in this study.

Restored Skull Model. FEA results for the restored skull model showed that the distribution of stress, strain, and displacement are highly variable for the three different bite scenarios and are strongly dependent on the bite position (Fig. 2 and *SI Appendix*, Figs. S1*A* and S2). The simulated bite at the tip of the snout recorded the lowest Von Mises stress, strain, and displacement, whereas the individual magnitudes significantly increased for the rostral- and caudal-bite scenarios. In the first load case (tip of the snout), peak stress and strain were restricted mainly to the premaxilla and the nasal, with maximum displacement found in the rostral snout region (Fig. 2*A*). With the shift of the bite point to the rostralmost (Fig. 2*E*) and successively to the caudalmost teeth (Fig. 2*I*), the skull roof (in particular, the frontals and the parietal) and the bones surrounding the antorbital fenestra displayed high stress and strain. Displacement is highest in the caudal-bite scenario and similarly affects the antorbital region, whereas the caudal part of the skull and the braincase showed no or only moderate displacement.

Rhamphotheca-Bearing models. The two skull models equipped with a keratinous rhamphotheca displayed a similar pattern of stress distribution to the restored skull model. Stress, strain, and displacement increase considerably with a more caudal biting position (Fig. 2 and *SI Appendix*, Fig. S2). In comparison with the restored skull model, however, individual magnitudes were generally lower in the models bearing a rhamphotheca (*SI Appendix*, Fig. S1*B*). In particular, the simulated bite scenario at the rhamphotheca-covered tip of the snout recorded lower Von Mises stresses and displacement, which is most pronounced in the model bearing the larger rhamphotheca (Figs. 2 and 3). For the caudal-bite scenario, the presence of a keratinous sheath did not mitigate stress and displacement, regardless of the extent to which the rhamphotheca covers the premaxilla or maxilla (Fig. 2 *J*, *K*, *V*, and *W*). Although overall stress and displacement were reduced in the two rhamphotheca models in both the bone and the keratinous material, strain was considerably increased within the keratinous structure itself when loaded directly, such as in the beak-bite scenarios. Underlying bone, however, showed reduced stress and strain (Fig. 3).

Dentigerous Model. The different bite simulations for the dentigerous model (that simulates the plesiomorphic presence of teeth in the edentulous premaxilla) largely followed the trend of the aforementioned models, with stress and strain values increasing with caudally shifting bite position (Fig. 2). As in the rhamphotheca-bearing scenarios, stress, strain, and displacement were mostly lower than in the restored skull model. Again, this stress-and-strain mitigating effect was lost for the caudal-bite scenarios, which showed a stress distribution pattern comparable to the restored skull model. The only exception was the model loaded at the first maxillary tooth, which shows highly increased displacement centered around the tip of the snout rostral to the bite point (Fig. 2*T*).

Lower Jaw Models. Compared with the simulations for the restored skull, the lower jaw model recorded considerably higher stress and strain magnitudes in all four bite scenarios than in the skull models (Fig. 4 and *SI Appendix*, Fig. S3). This trend was to be expected, as the mandibles transmit the bulk of the muscle forces and are thus more strongly affected by the generated bite forces. Stress, strain, and displacement increased as the bite point

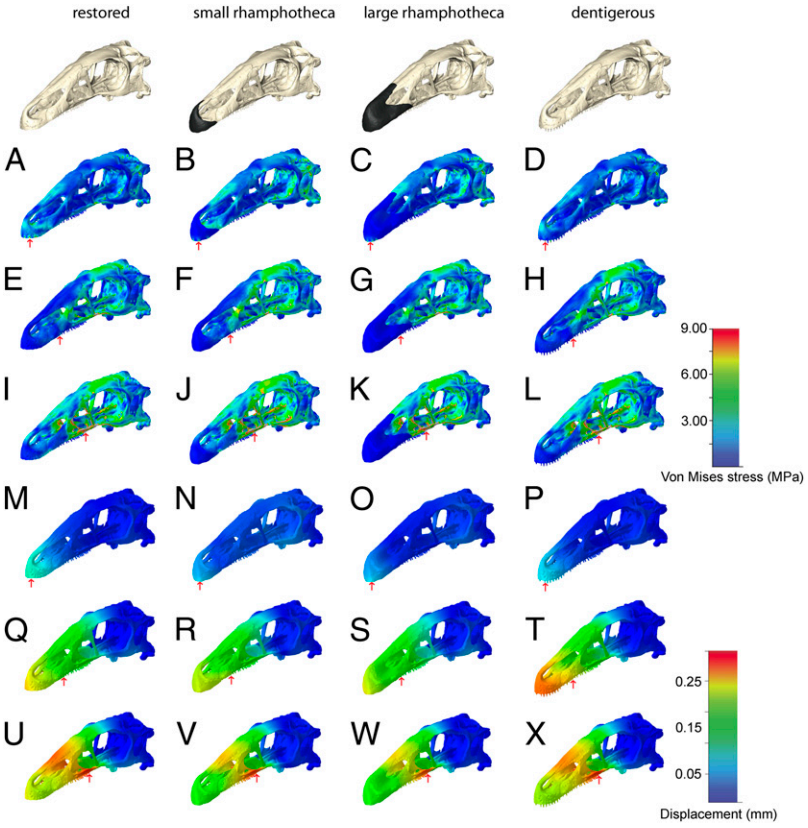

Fig. 2. Comparisons of (*A–L*) Von Mises stress and (*M–X*) displacement distribution in the different skull configurations of *E. andrewsi* subjected to different bite positions. Each of the four columns presents a different modeled state, from left, restored skull, with small rhamphotheca, with large rhamphotheca, with teeth added to the premaxillae and maxillae. The rows depict different bite positions (indicated by red arrows). Contour plots are scaled to (*A–L*) 9-MPa peak stress and (*M–X*) 0.25-mm displacement.

shifted caudally. Peak stress and strain occurred primarily in the caudal region of the mandible (surangular, prearticular, angular) and the caudal portion of the dentary. The highest magnitudes (stress, strain, and displacement) were found in the bite scenario loading the fifth dentary tooth, which forms the counterpart to the first maxillary tooth (Fig. 4 *C* and *K*). The caudalmost bite point, however, appeared to affect mainly the caudal region of the mandible, leaving the dentary relatively unstressed (Fig. 4 *D* and *L*). Unlike in the skull models, the attachment of a keratinous sheath to the lower jaw had nearly no effect on mitigating stress or strain (Fig. 4 *E–H* and *M–P*).

Neck Muscles. The bite scenarios incorporating an interaction between the jaw adductor and the neck muscles in simulation of a pull-back motion, displayed among the lowest stress and strain magnitudes for all tested loading scenarios (Fig. 5). The magnitudes are comparable with the beak-bite scenarios for the restored skull model and the rhamphotheca models, although the distribution of stress, strain, and displacement is more homogenous in the neck muscle models. In the latter, peak stress and strain centered around the skull roof and the lateral braincase walls (Fig. 5 *A* and *E*). In the models incorporating a rhamphotheca, strain magnitudes were increased in the keratinous material (Fig. 5 *B* and *F*).

It is noteworthy that the bite scenarios for the neck muscles alone resulted in higher peak stress and strain in the skull roof (Fig. 5 *D* and *H*). Displacement was similarly increased compared with the combined loading of the adductor and neck musculature.

Discussion

The results of our FEA models show that peak stress and displacement demonstrably increase with the shifting of the bite location from the edentulous part of the snout to the caudally located tooth-bearing elements. Although bite forces are relatively low in *E. andrewsi* compared with other (carnivorous) theropods (18–20), these forces have a considerable effect on the distribution of stress in the cranial skeleton. Although care should be taken when relying on absolute values derived from FEAs (21), the comparative context of the different bite scenarios clearly shows that the cranial structure would have had to withstand increased stress and strain in each of the tooth-biting scenarios. The absence of wear facets on the individual teeth of *E. andrewsi*, the lack of tooth occlusion between the maxilla and the dentary, and the low tooth-replacement rate in *E. andrewsi*, particularly in the caudal part of the tooth row of the maxilla and the dentary (17), suggest that biting and food processing were most likely restricted to the edentulous tip of the snout, rather than active mastication involving teeth—a finding consistent with the results of the FEAs presented herein.

In other theropod clades, and in fact in most dinosaur groups in general (22, 23), tooth loss is usually accompanied by the development of a rostral beak (24–26). Both FE models incorporating such a structure in the *Erlikosaurus* skull models demonstrate that the presence of a keratinous sheath would help to reduce Von Mises stress and strain in the underlying bone. Although strain (both maximum and minimum principal strain) is increased in the rhamphotheca itself, the softer keratin sheath mitigates strain better (10) than does the more brittle bone, protecting the latter from fracturing. This effect is most notable for the bite simulations at the tip of the snout and the rhamphotheca, whereas stress and strain distribution and magnitude are unaffected in the caudal biting scenarios. Regardless of the size of the rhamphotheca, displacement is noticeably reduced in all modeled bite scenarios where a rhamphotheca is present.

In this context, it is worth noting that the hypothetical, fully dentigerous model in this study also recorded lower stress, strain, and displacement magnitudes in the premaxilla. This result is not completely unexpected, given that the thickness of the respective bone was artificially increased. However, in comparison with the

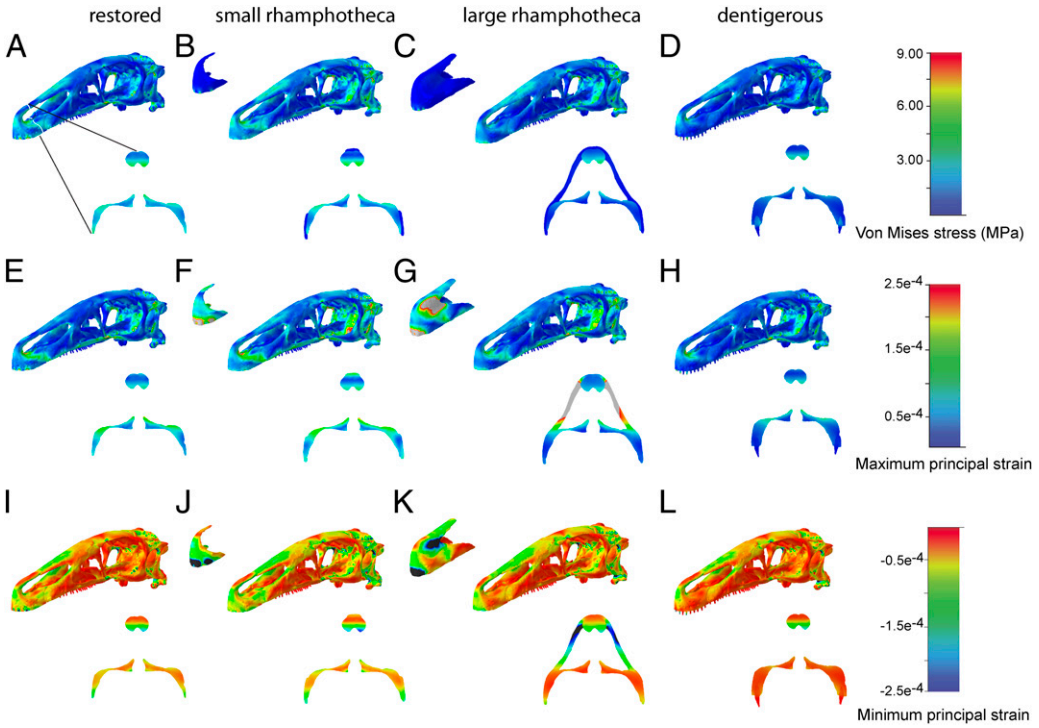

Fig. 3. Comparison of (*A–D*) Von Mises stress, (*E–H*) maximum principal strain, and (*I–L*) minimum principal strain distribution in the different skull configurations of *E. andrewsi* and coronal cross-sections through the premaxillary region. All models simulate a bite at the tip of the beak. Contour plots are scaled to (*A–D*) 9-MPa peak stress, (*E–H*) 0.00025 peak strain, and (*I–L*) −0.00025 peak strain.

rhamphotheca models, the stress-mitigating effects are only localized to the reinforced elements of the snout and are more prone to displacement. Furthermore, rather than dissipating stress and strain, the increase in thickness of an isolated structure could also result in elevating stress and strain magnitudes (27) in other (adjacent) elements, as probably occurred in the model simulating a bite at the fifth maxillary tooth (Fig. 2*T*).

In contrast to the skull, the lower jaw models are more sensitive to stress and strain, which is concentrated in the caudal part of the mandible. This sensitivity appears to be a direct result of the adductor muscles acting on the insertion points. Although the presence of a large patent suture at the intramandibular fenestra was not incorporated into the model, it would have no effect on the elements bearing the muscle attachment sites, as it is located rostral to the muscle insertions.

However, due to its geometric arrangement, the rostral tip of the snout produced the lowest bite forces in *Erlikosaurus* (18). Assuming that food processing was restricted to the edentulous part of the snout, *Erlikosaurus* would have had only used a fraction of the available muscle force when cropping vegetation. Such low bite forces might not have been sufficient to bite through thicker foliage and food particles (28). Feeding mechanisms in several other (carnivorous) theropods involve the interaction between the jaw adductors and the cervical musculature (20, 29, 30), and it appears likely that *E. andrewsi* could have harnessed the neck muscles in a similar way to compensate for the low bite forces without notably increasing cranial stress at the same time. Even though estimated adductor muscle are considerably higher than the maximal possible bite forces (*SI Appendix*, Table S4), results of our FEAs show that such a muscle-driven neck-pull mechanism would cause only minimal additional stress

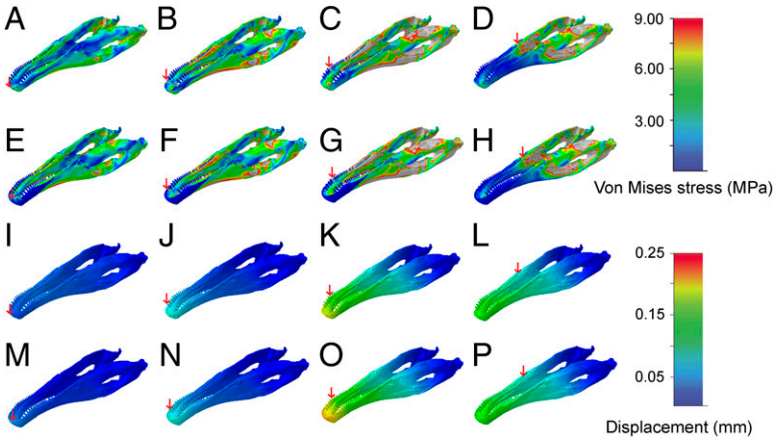

Fig. 4. Comparisons of (*A–H*) Von Mises stress and (*I–P*) displacement distribution in the different jaw models of *E. andrewsi*. (*A–D* and *I–J*) restored lower jaw model and (*E–H* and *M–P*) restored lower jaw with rhamphotheca. Each column presents a different bite positions (indicated by red arrows). Contour plots are scaled to (*A–H*) 9-MPa peak stress and (*I–P*) 0.25-mm displacement.

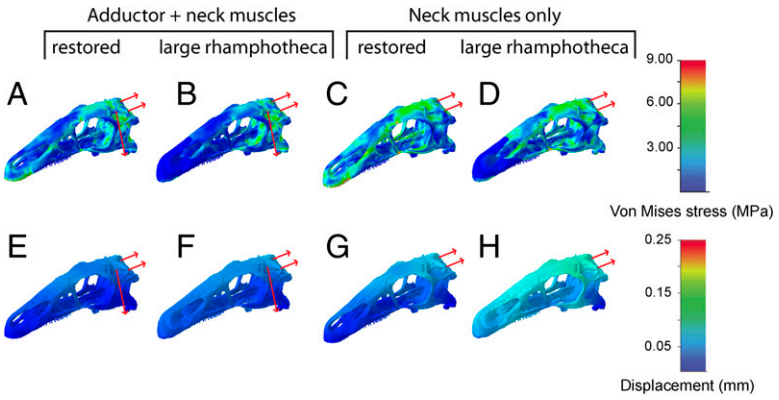

Fig. 5. Comparisons of (*A–D*) Von Mises stress and (*E–H*) displacement distribution for different muscle interactions in *E. andrewsi*. Contour plots are scaled to (*A–D*) 9-MPa peak stress and (*E–H*) 0.25-mm displacement.

and strain across the cranial skeleton, as long as the adductor muscles are contracting. However, the action of the cervical musculature alone would result in increased cranial stress and necessitates the tension of the adductor musculature to provide an antagonistic bracing system. Phylogenetically constrained by a general theropod bauplan, *Erlikosaurus*, and presumably also other maniraptoriform taxa, could have harnessed the postcranial musculature to compensate for the relatively low bite forces and meet the functional demands of cropping foliage and stripping leaves of branches, thus adapting an inherited morphological and functional system for modified ecological demands.

In Avialae, tooth loss, paralleled by beak development, is generally assumed to represent a response to the requirement for weight reduction to enable flight (9, 31). However, the results for *E. andrewsi* indicate that weight (mass) saving was only minimal (*SI Appendix*, Table S1) and that a more extensive rhamphotheca would actually have increased the weight (mass) of the cranium. Rather, the development of a keratinous rhamphotheca lowers cranial stress and strain and could also have served the purpose of increasing cranial stability and thus flexibility. As such, keratinous beaks are lightweight in terms of their strength-to-weight ratio, even though their actual weight might be greater than that of teeth (32). Derived bird beaks circumvent this problem, as a potential increase in weight is compensated for by the reduction in volume or thickness in the underlying bones or specialized lightweight structures (9, 11).

Evidence, from both this biomechanical study and the osteology (lack of wear facets, tooth occlusion, tooth replacement) of *Erlikosaurus*, suggests that the tip of the snout (i.e., edentulous premaxilla plus overlying rhamphotheca) was used as the main device to procure and process food. The presence of a keratinous rhamphotheca in this region would have helped to dissipate and absorb stress and strain while making the snout less susceptible to bending and displacement. As an ever-growing material, keratin has the advantage over bone that it is able to rapidly repair fractures and has a slower crack propagation rate, thus reducing the risk of constant damage (33).

Basal taxa in various maniraptoriform lineages display functional analogs to a rostral beak formed by the premaxillary teeth (4, 34, 35). This fact might indicate that basal members in various groups experimented with various teeth configurations to create a more beak-like cutting surface. Such a design would functionally be more favorable than discrete tooth elements, particularly as these beak analogs would have to perform a different function in herbivores. This trend further corroborates the possibility that the rostral region of the skull played an essential role in food gathering for these taxa, which was then replaced by a keratinous structure in the course of evolution.

However, this has even further, macroevolutionary implications and the functional and ecological transition occurring in Maniraptoriformes. Nearly all basal avialans are considered to be herbivorous, and various phylogenetic analyses have recovered this group outside of Deinonychosauria (36, 37), which potentially had reacquired carnivory secondarily. This fact would not only make herbivory but also the appearance of edentulism and keratinous beaks homologous throughout the lineage leading up to basal Avialae. Similar to the evolution of feathers, beaks might not necessarily have served the same function in nonavian theropods as they do in extant birds—namely the additional advantage of weight reduction for flight—but rather to reduce stress and strain in the cranial skeleton. Apart from birds, edentulism and beaks have appeared in multiple lineages in tetrapod history, all of which do not fly.

Materials and Methods

Skull Models and Digital Reconstruction. The digitally restored model of the skull and lower jaw of *E. andrewsi* are based on CT scans of the original specimens (IGM 100/111; Geological Institute of the Mongolian Academy of Sciences, Ulaan Bataar, Mongolia), performed at X-Tek Systems (now Nikon Metrology). The specimens were scanned with a XT-H-225ST CT scanner, set at 180 kV and 145 μA for the complete skull and lower jaw. The resulting rotational projections were processed with custom built software provided by X-Tek Systems, creating VGI and VOL files, which contain 1,998 slices with a slice thickness of 145 μm for the complete skull the lower jaw. The final slice datasets were imported into Avizo (Versions 6.3.1. and 7.0.0 VSG; Visualization Science Group) for image segmentation and digital reconstruction.

Although the skull and lower jaw of *E. andrewsi* are well preserved and mostly complete, the digital model required moderate reconstruction to accurately represent the inferred life morphology. To achieve this, each individual element of the specimen was separately labeled and isolated using Avizo's segmentation editor. Where necessary, breaks and cracks were digitally removed, and distortions or deformations were digitally corrected. For the last step, the individual cranial elements were reassembled and articulated into the final model, following a protocol outlined in ref. 18. The restored model bears 24 teeth in the maxilla and 32 in the dentary. The premaxilla and the ultimate tip of the dentary are edentulous (17, 18).

In addition to the restored skull configuration, two (hypothetical) skull models and a lower jaw model bearing a keratinous rhamphotheca were created in Avizo. A keratinous layer of ~3 mm thickness was modeled. The different morphologies of the rhamphothecae on the skull bracket the different interpretations of osteological correlates and cover the underlying bones to varying extents (*SI Appendix*, Fig. S4).

Among the individual maniraptoriform lineages, the basalmost taxa are characterized by an increased number of teeth in the premaxilla and maxilla and/or a marked heterodonty (34, 38). Due to the lack of preserved cranial remains, information on the basal condition in Therizinosauria is unavailable. Thus, a further hypothetical model was created in Avizo, using the restored model of *E. andrewsi* as a template, incorporating teeth in the premaxilla and the maxilla to simulate a phylogenetically more basal, fully dentigerous condition, whereas the remaining parts of the osteology remained unchanged. This model has three additional teeth in each maxilla and seven teeth in the premaxilla. The respective teeth were duplicated from preserved rostral teeth in the maxilla. The thicknesses of the bone regions bearing these modeled teeth were increased in accordance with regions with preserved teeth.

Adductor Musculature and Bite Force. To gain reliable and approximately accurate values for the muscle and bite force calculations (*SI Appendix*, Table S3), the adductor musculature of *E. andrewsi* was digitally reconstructed in Avizo. 3D reconstructions of each muscle were created based on osteological correlates of the original specimen and the restored skull model, respectively, as well as topological and neurovascular criteria. For a detailed description of the muscle reconstruction process, see ref. 20.

Due to the lack of preserved elements, the full extent of the neck musculature could not be reconstructed accurately. The muscle force estimates for the respective model are thus based on generalized muscle attachment sites at the back of the skull only (*SI Appendix*, Fig. S5).

FEA. The different surface models of the skull and lower jaw of *E. andrewsi* were imported into Hypermesh (Versions 10 and 11; Altair Engineering) to create solid mesh FE models, consisting of ∼2,000,000 four-noded tetrahedral elements (tet4) for the skull models and 1,000,000 elements for the lower jaw models (for details, see *SI Appendix*, Table S1). Convergence and sensitivity tests were performed to gauge accuracy and variation for different model sizes and element types. For the two models bearing a rhamphotheca, the keratinous layer was attached directly to the bone, so that both materials share nodes along the contact zone. Although the rhamphotheca of modern birds forms a complex, multilayer structure, here it was modeled as a single, homogenous isotropic layer connected via shared nodes to the bone. Validation experiments on the beaks of extant finches have shown that these assumptions yield high correlations between ex vivo experimental displacements and displacements from skull and beak FE models ($R^2 = 0.97$ for loading at the anterior rostrum, $R^2 = 0.89$ loading elsewhere along the beak). Thereby our methodology for FE model construction can be considered valid and biologically realistic (10).

Material properties were assigned in Hypermesh for three different tissue types, which were treated as isotropic and homogenous: cranial bone, enamel, and keratin. In the absence of exact material properties for fossil bone, enamel, and keratin, extant analogs for alligator mandibles ($E = 20.49$ GPa, $\upsilon = 0.40$) (39), crocodile teeth ($E = 60.40$ GPa, $\upsilon = 0.31$) (40), and bird beaks ($E = 1.04$ GPa, $\upsilon = 0.40$) (41) were used. The skull models were constrained from rigid body motion in all directions (X,Y,Z) at the occipital condyle (six nodes), the condyles of the mandibular capitulum of the quadrates (seven nodes on each side), and (with the exception of the neck muscle models) the paroccipital processes (seven nodes on each side), reflecting attachment to the vertebral column, the lower jaw, and the cranial musculature. The models for the lower jaws were constrained at the glenoid region (nine nodes on each side; compare also *SI Appendix*, Tables S1–S3).

All models were imported into Abaqus (Version 6.10; Simulia) for analysis and postprocessing. Three different sets of linear simulations were solved for each of the skull models: (*i*) simulated bilateral biting at the tip of the snout with constraints (simulating the bite point) applied at five nodes along the rostroventral margin of the premaxilla or the rhamphotheca respectively (for the model bearing teeth in the premaxilla, constraints were applied to the two rostralmost teeth on each side); (*ii*) simulated bilateral biting at the first maxillary tooth on each side; and (*iii*) simulated bilateral biting on the last maxillary tooth on each side. For the lower jaw models, bilateral biting was simulated at (*i*) the tip of the dentary or the rhamphotheca with constraints applied to five nodes; (*ii*) the first dentary tooth on each side; (*iii*) the fifth dentary tooth on each side, as this tooth position occludes with the first maxillary tooth; and (*iv*) the last dentary tooth on each side. Bite points parallel the calculated bite forces for *E. andrewsi* in ref. 18. Additional simulations were solved incorporating the neck musculature: (*i*) adductor and neck muscles and (*ii*) neck muscles only.

ACKNOWLEDGMENTS. We thank Andrew Ramsey and Mike Robinson (Nikon Metrology) for support with the scanning of *Erlikosaurus*. Jen Bright and Imran Rahman (University of Bristol) provided helpful discussions and advice, which improved earlier versions of the manuscript. This work is supported by a doctoral fellowship to S.L. by the Volkswagen Foundation, Germany.

1. Sereno PC (1997) The origin and evolution of dinosaurs. *Annu Rev Earth Planet Sci* 25(1):435–489.
2. Padian K, Chiappe LM (1998) The origin and early evolution of birds. *Biol Rev Camb Philos Soc* 73(1):1–42.
3. Makovicky PJ, Zanno LE (2011) Theropod diversity and the refinement of avian characteristics. *Living Dinosaurs*, eds Dyke G, Kaiser G (John Wiley & Sons, New York), pp 9–29.
4. Zanno LE, Makovicky PJ (2011) Herbivorous ecomorphology and specialization patterns in theropod dinosaur evolution. *Proc Natl Acad Sci USA* 108(1):232–237.
5. Barrett PM (2005) The diet of ostrich dinosaurs (Theropoda: Ornithomimosauria). *Palaeontology* 48(2):347–358.
6. Barrett PM, Rayfield EJ (2006) Ecological and evolutionary implications of dinosaur feeding behaviour. *Trends Ecol Evol* 21(4):217–224.
7. Zanno LE, Gillette DD, Albright LB, Titus AL (2009) A new North American therizinosaurid and the role of herbivory in 'predatory' dinosaur evolution. *Proc R Soc Lond Ser B* 276(1672):3505–3511.
8. Davit-Béal T, Tucker AS, Sire JY (2009) Loss of teeth and enamel in tetrapods: Fossil record, genetic data and morphological adaptations. *J Anat* 214(4):477–501.
9. Louchart A, Viriot L (2011) From snout to beak: The loss of teeth in birds. *Trends Ecol Evol* 26(12):663–673.
10. Soons J, et al. (2012) Multi-layered bird beaks: A finite-element approach towards the role of keratin in stress dissipation. *J R Soc Interface* 9(73):1787–1796.
11. Seki Y, Mackey M, Meyers MA (2012) Structure and micro-computed tomography-based finite element modeling of Toucan beak. *J Mech Behav Biomed Mater* 9:1–8.
12. Zanno LE (2010) A taxonomic and phylogenetic re-evaluation of Therizinosauria (Dinosauria: Maniraptora). *J Syst Palaeontol* 8(4):503–543.
13. Russell DA, Dong Z (1993) The affinities of a new theropod from the Alxa-Desert, Inner Mongolia, People's Republic of China. *Can J Earth Sci* 30(10):2107–2127.
14. Xu X, Wang X-l (1999) A therizinosauroid dinosaur with integumentary structures from China. *Nature* 399(6734):350–354.
15. Perle A (1981) A new segnosaurid from the Upper Cretaceous of Mongolia. *Joint Soviet-Mongolian Paleontol Expedition Trans* 8(15):45–55.
16. Gillette DD (2007) Therizinosaur: Mystery of the sickle-clawed dinosaur. *Plateau: Land and People of the Colorado Plateau* 4(2):1–69.
17. Clark JM, Perle A, Norell MA (1994) The skull of *Erlicosaurus andrewsi*, a Late Cretaceous "Segnosaur" (Theropoda: Therizinosauridae) from Mongolia. *Am Mus Novit* 3115:1–39.
18. Lautenschlager S (2013) Cranial myology and bite force performance of *Erlikosaurus andrewsi*: A novel approach for digital muscle reconstructions. *J Anat* 222(2):260–272.
19. Erickson GM, et al. (1996) Bite-force estimation for *Tyrannosaurus rex* from tooth-marked bones. *Nature* 382(6593):706–708.
20. Rayfield EJ, et al. (2001) Cranial design and function in a large theropod dinosaur. *Nature* 409(6823):1033–1037.
21. Bright JA, Rayfield EJ (2011) Sensitivity and ex vivo validation of finite element models of the domestic pig cranium. *J Anat* 219(4):456–471.
22. Papp MJ, Witmer L (1998) Cheeks, beaks or freaks: A critical appraisal of buccal soft-tissue anatomy in ornithischian dinosaurs. *J Vertebr Paleontol* 18(3):69A.
23. Czerkas S (1999) The beaked jaw of stegosaurs and their implications for other ornithischians. *Vertebrate Paleontology in Utah*, ed Gillette DD (Utah Geological Survey, Salt Lake City), Vol 99, pp 143–150.
24. Norell MA, Makovicky PJ, Currie PJ (2001) Palaeontology. The beaks of ostrich dinosaurs. *Nature* 412(6850):873–874.
25. Kobayashi Y, Barsbold R (2005) Reexamination of a primitive ornithomimosaur, *Garudimimus brevipes* Barsbold, 1981 (Dinosauria: Theropoda), from the Late Cretaceous of Mongolia. *Can J Earth Sci* 42(9):1501–1521.
26. Hieronymus T, Witmer LM (2010) Homology and evolution of avian compound rhamphothecae. *Auk* 127(3):590–604.
27. Richmond BG, et al. (2005) Finite element analysis in functional morphology. *Anat Rec A Discov Mol Cell Evol Biol* 283(2):259–274.
28. Reichel M (2010) A model for the bite mechanics in the herbivorous dinosaur *Stegosaurus* (Ornithischia, Stegosauridae). *Swiss J Geosci* 103(2):235–240.
29. Snively E, Russell AP (2007) Functional morphology of neck musculature in the Tyrannosauridae (Dinosauria, Theropoda) as determined via a hierarchical inferential approach. *Zool J Linn Soc* 151(4):759–808.
30. Mazetta GV, Cisilino AP, Blanco RE, Calvo N (2009) Cranial mechanics and functional interpretations of the horned carnivorous dinosaur *Carnotaurus sastrei*. *J Vertebr Paleontol* 29(3):822–830.
31. Zhou Z, Li FZZ (2010) A new Lower Cretaceous bird from China and tooth reduction in early avian evolution. *Proc R Soc B Biol Sci* 277(1679):219–227.
32. Dumont ER (2010) Bone density and the lightweight skeletons of birds. *Proc Biol Sci* 277(1691):2193–2198.
33. Homberger DG, Brush AH (1986) Functional-morphological and biochemical correlations of the keratinized structures in the African Grey Parrot, *Psittacus erithacus* (Aves). *Zoomorphology* 106(2):103–114.
34. Perez-Moreno BP, et al. (1994) A unique multitoothed ornithomimosaur dinosaur from the Lower Cretaceous of Spain. *Nature* 370(6488):363–367.
35. Ji Q, Currie PJ, Norell MA, Shu-An J (1998) Two feathered dinosaurs from northeastern China. *Nature* 393(6687):753–761.
36. Xu X, You H, Du K, Han F (2011) An *Archaeopteryx*-like theropod from China and the origin of Avialae. *Nature* 475(7357):465–470.
37. Xu X, Pol D (2013) *Archaeopteryx*, paravian phylogenetic analyses, and the use of probability-based methods for palaeontological datasets. *J Syst Palaeontology* 1–12.
38. Balanoff AM, Xu X, Kobayashi Y, Matsufune Y, Norell MA (2009) Cranial osteology of the theropod dinosaur *Incisivosaurus gauthieri* (Theropoda: Oviraptorosauria). *Am Mus Novit* 3651:1–35.
39. Zapata U, et al. (2010) Material properties of mandibular cortical bone in the American alligator, *Alligator mississippiensis*. *Bone* 46(3):860–867.
40. Creech JE (2004) Phylogenetic character analysis of crocodylian enamel microstructure and its relevance to biomechanical performance. MS thesis (Florida State Univ, Tallahassee, FL).
41. Chen P-Y, et al. (2008) Structure and mechanical properties of selected biological materials. *J Mech Behav Biomed Mater* 1(3):208–226.

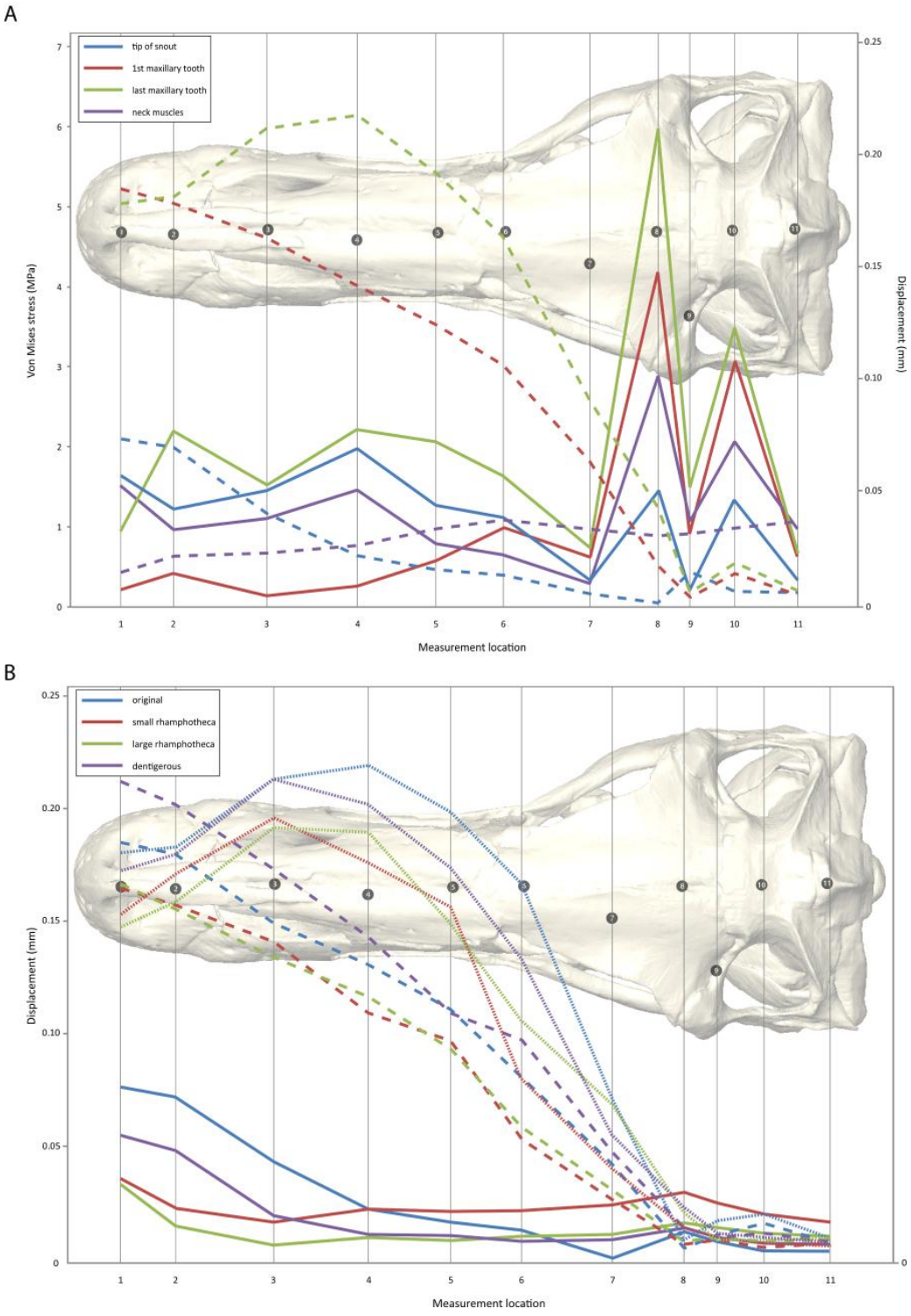

Fig. S1. (*A*) Von Mises stress (solid lines) and displacement (stippled lines) magnitudes in the restored skull model for four different bite scenarios along eleven distinct measurement locations (aligned with the respective position on the skull in the background, comp Table S5). (*B*). Displacement in the four different skull configurations for simulated bite at the tip of the snout (solid lines), the first maxillary tooth (large stippled lines), and the last maxillary tooth (small stippled lines).

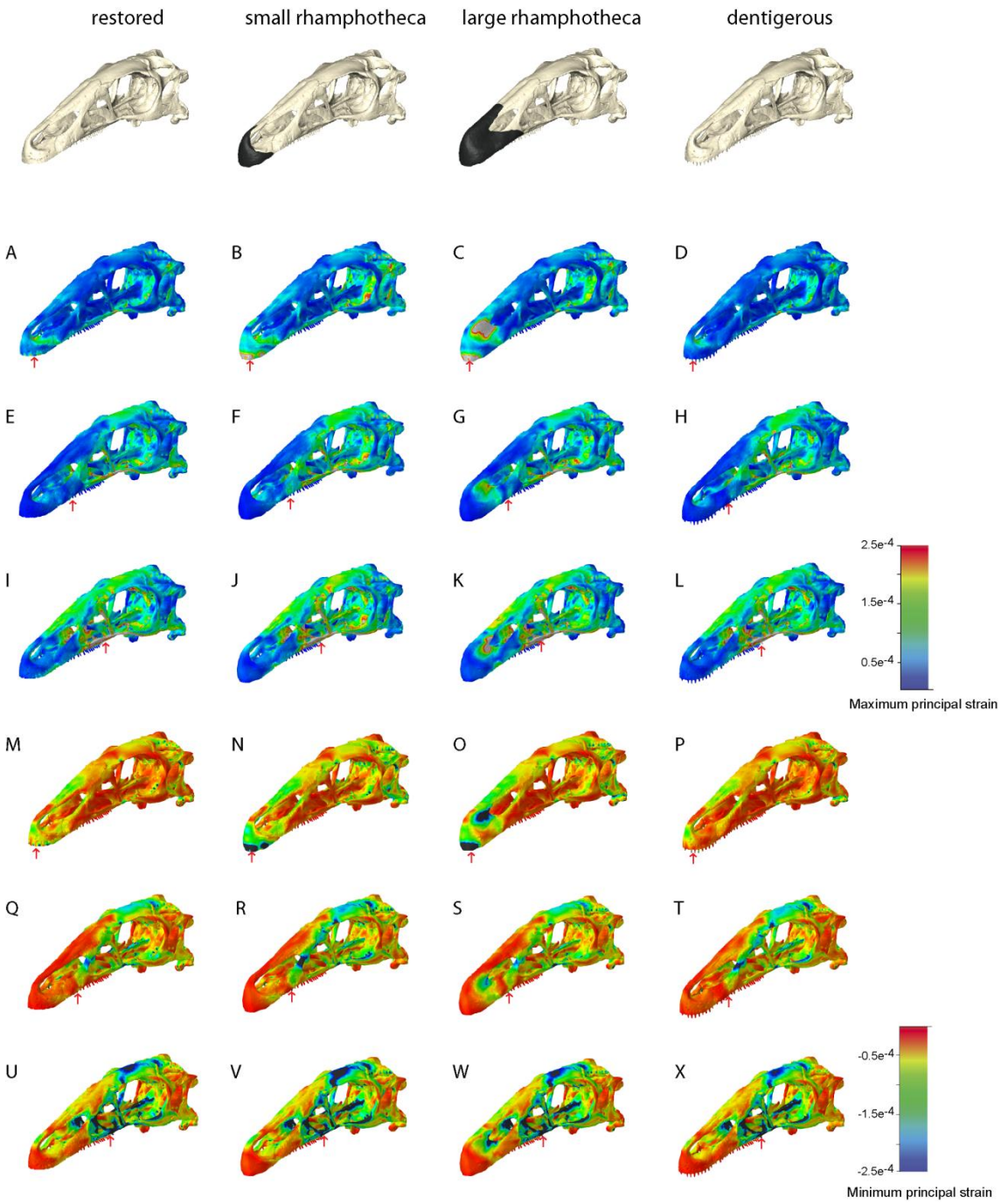

Fig. S2. Comparisons of (*A–L*) Maximum principal strain and (*M–X*) Minimum principal strain distribution in the different skull configurations of *Erlikosaurus andrewsi* subjected to different bite positions. Each of the four columns presents a different modeled state, from left, restored skull, with small rhamphotheca, with large rhamphotheca, with teeth added to the premaxillae and maxillae. The rows depict different bite positions (indicated by red arrows). Contour plots are scaled to (A–C) 0.00025 peak strain and (D-F) -0.00025 peak strain.

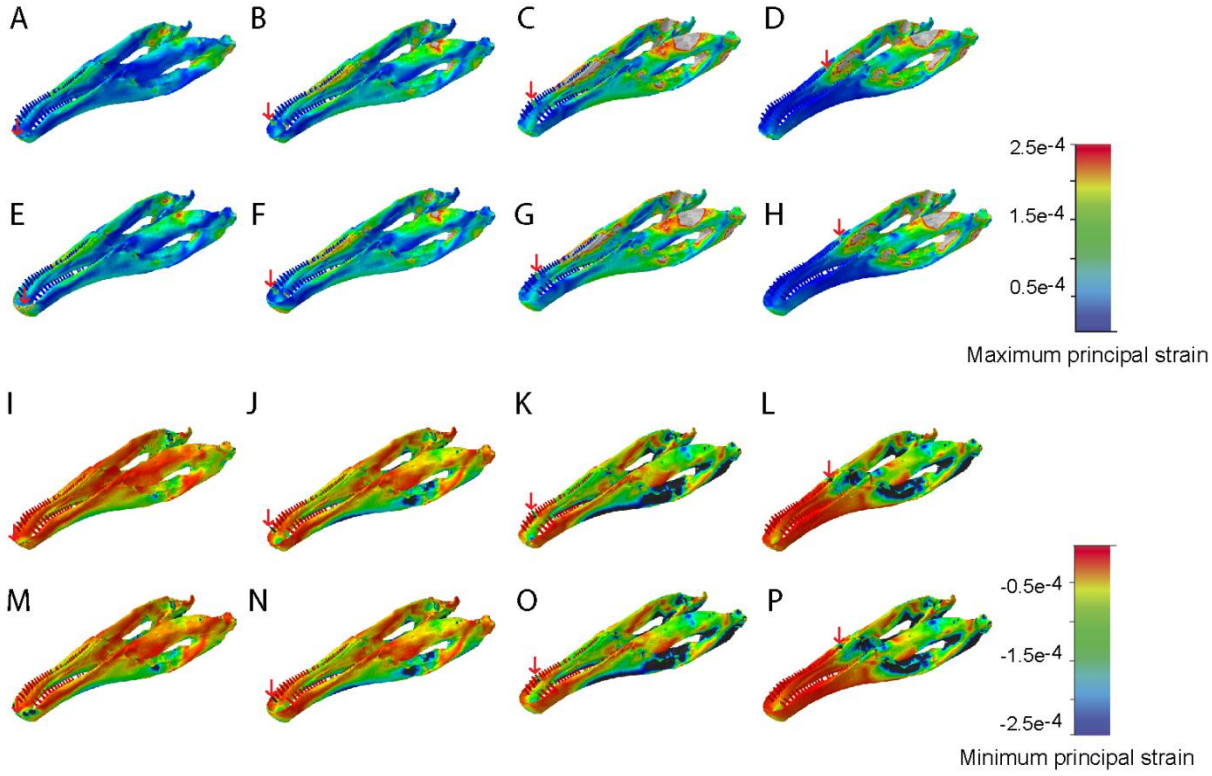

Fig. S3. Comparisons of (*A–H*) Maximum principal strain and (*I–P*) Minimum principal strain distribution in the different jaw models of *Erlikosaurus andrewsi*. (*A–D*, *I–J*) restored lower jaw model, (*E–H*, *M–P*) restored lower jaw with rhamphotheca. Each column presents a different bite positions (indicated by red arrows). Contour plots are scaled to (*A–H*) 9 MPa peak stress and (*I–P*) 0.25 mm displacement.

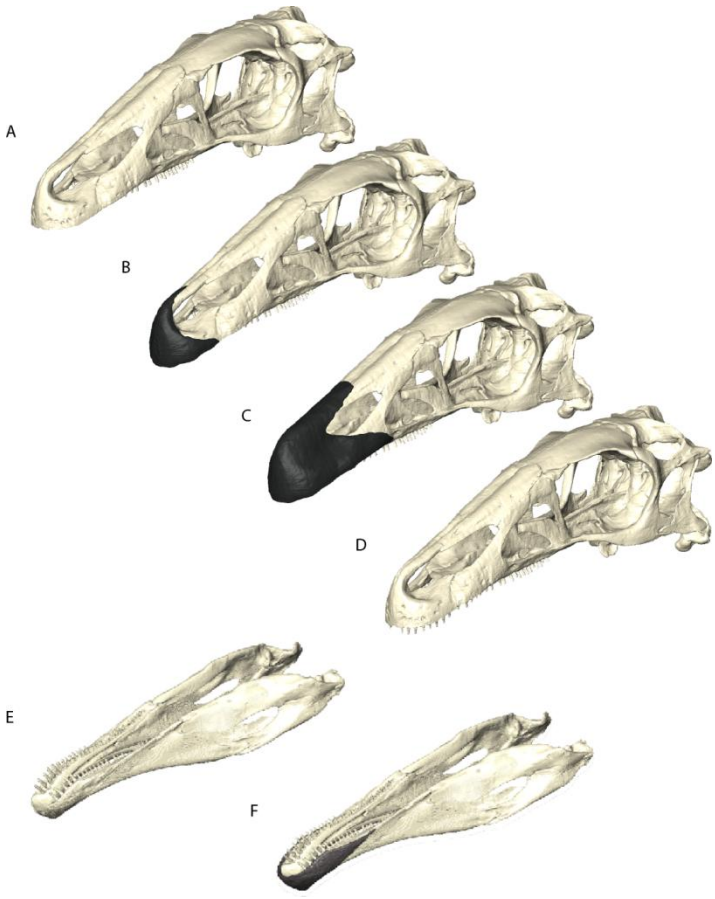

Fig. S4. Different skull configurations of *Erlikosaurus andrewsi*. (*A*) restored skull, (*B*) skull with small rhamphotheca, (*C*) skull with large rhamphotheca, (*D*) skull with teeth added to the premaxilla and maxilla, (*E*) restored lower jaw, (*F*) lower jaw with rhamphotheca.

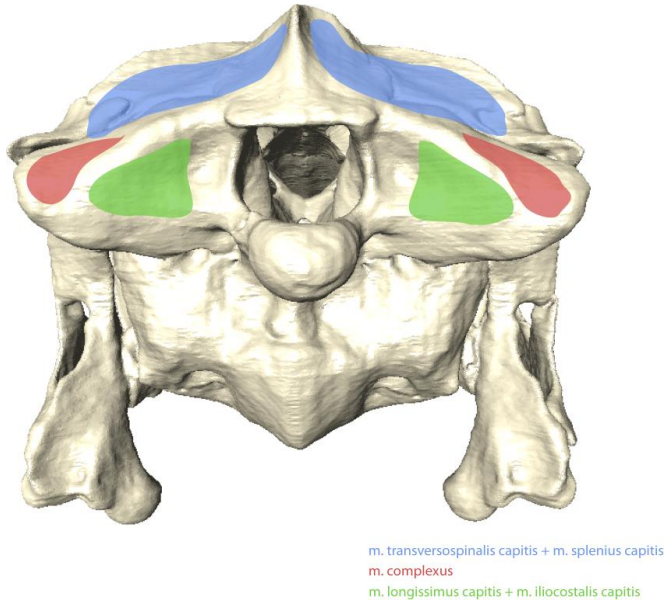

Fig S5. Generalized attachment sites of the neck musculature for muscle force calculations (Table S4).

Model	Number of elements	Surface area [mm²]	Mass [g]
Restored skull	1 905 393	124 815	360
Restored skull with small rhamphotheca	1 921 002	126 117	365
Restored skull with large rhamphotheca	1 989 380	128 897	374
Restored skull, fully dentigerous model	1 961 098	125 418	368
Lower jaw	1 007 423	60 560	107
Lower jaw plus rhamphotheca	1 077 317	62 972	111
Premaxillary & maxillary teeth	-	-	3
Small rhamphotheca (skull only)	-	-	5
Large rhamphotheca (skull only)	-	-	15

Table S1. Size (number of elements, surface area, calculated mass) of the individual FE models. The weight of the individual models and components (Table S1) was calculated by using volumetric measurements for single components and specific densities for bone (1770 kg/m^3), teeth (2076 kg/m^3), and keratin (1269 kg/m^3).

#	Model	Loaded forces		Constraints			Constraints simulating bite process		
	Skull	Adductor muscles	Neck muscles	Occipital condyle	Paroccipital process	Quadrate	Tip of snout	1st maxillary tooth	Last maxillary tooth
1	restored	X		X	X	X	X		
2	restored	X		X	X	X		X	
3	restored	X		X	X	X			X
4	small rhamphotheca	X		X	X	X	X		
5	small rhamphotheca	X		X	X	X		X	
6	small rhamphotheca	X		X	X	X			X
7	large rhamphotheca	X		X	X	X	X		
8	large rhamphotheca	X		X	X	X		X	
9	large rhamphotheca	X		X	X	X			X
10	dentigerous	X		X	X	X	X		
11	dentigerous	X		X	X	X		X	
12	dentigerous	X		X	X	X			X
13	restored	X	X	X		X	X		
14	restored		X	X		X	X		
15	large rhamphotheca	X	X	X		X	X		
16	large rhamphotheca		X	X		X	X		

Table S2. Model setup for different tested FE models of the skull of *Erlikosaurus andrewsi* presented in this study.

#	Model	Loaded forces	Constraints	Constraints simulating bite process			
	Lower jaw	Adductor muscles	Glenoid	Tip of dentary	1st dentary tooth	5th dentary tooth	Last dentary tooth
17	Lower jaw	X	X	X			
18	Lower jaw	X	X		X		
19	Lower jaw	X	X			X	
20	Lower jaw	X	X				X
21	Lower jaw + rhamphotheca	X	X	X			
22	Lower jaw + rhamphotheca	X	X		X		
23	Lower jaw + rhamphotheca	X	X			X	
24	Lower jaw + rhamphotheca	X	X				X

Table S3. Model setup for different tested FE models of the lower jaw of *Erlikosaurus andrewsi* presented in this study.

Muscle	Muscle force [N]
Adductor muscles (muscle forces per side)	
m. pterygoideus dorsalis	55.94
m. pterygoideus ventralis	182.15
pseudotemporalis profundus	13.49
m. pseudotemporalis superficialis	44.76
m. adductor mandibulae externus profundus	78.11
m. adductor mandibulae externus medialis	76.80
m. adductor mandibulae externus superficialis	83.22
adductor mandibulae posterior	34.86
Cervical muscles (combined for left and right side)	
m. transversospinalis capitis + m. splenius capitis	600
m. complexus	500
m. longissinus capitis + m. iliocostalis capitis	600

Table S4. Calculated muscle forces for the adductor and neck musculature.

Measurement location	Description
1	Nasal process of premaxilla, rostrally
2	Nasal process of premaxilla, caudally
3	Nasal/premaxilla contact
4	Dorsal surface of nasal
5	Nasal/frontal contact
6	Dorsal surface of frontal, rostrally
7	Laterodorsal surface of frontal
8	Frontal/parietal contact
9	Frontal/postorbital contact
10	Dorsal surface of parietal
11	Parietal/supraoccipital contact

Table S5. Location of measurement sites along the skull of *Erlikosaurus andrewsi* as shown in Fig S1.